Mineralium Deposita (2024) 59:69–83
https://doi.org/10.1007/s00126-023-01200-z

ARTICLE

Morphology and structural evolution of fine beach gold in comparison to detrital platinum, southern New Zealand

Marshall Palmer[1] · **Dave Craw**[1]

Received: 13 February 2023 / Accepted: 31 July 2023 / Published online: 9 August 2023

Abstract

Beach placer gold has been mined around the world historically, but extraction of fine (~ 100 µm) gold particles is notoriously difficult. This study illustrates morphological and mineralogical changes that transform fine gold during aeolian processes on windy beaches and contribute to mine concentration inefficiencies. Sandblasting on exposed beaches in southern New Zealand has caused extreme attenuation of edges of gold flakes that were previously transported in rivers for > 200 km. Flakes have been transformed into complex but compact toroids and spheroids with thin (~ 20 µm) internal and external strands of attenuated gold. Most of the gold within the attenuated strands has recrystallised to fine (micron-scale) undeformed grains with little or no Ag (< 1 wt%). Some coarse (> 40 µm) gold grains remain from the precursor fluvial particles, and these retain original Ag contents (1–10 wt%). These coarse grains show substantial internal crystallographic deformation and sub-grain formation, although some of these strain effects may have been inherited from fluvial transport. Co-existing detrital platinum minerals are much less malleable than gold during sandblasting and have only minor (10-µm scale) toroidal deformation on edges of fluvial flakes. The complex frameworks of the fine toroidal and spheroidal gold particles can include air, water, and clay, which lowers their average density and so they commonly float on water and are readily entrained with other heavy minerals. The fine particle size, compact shapes, and clay coatings also resist mercury amalgamation.

Keywords Gold · Placer · Beach · Aeolian · Toroid · Platinum · Deformation

Introduction

Detrital gold particles in sedimentary systems can provide useful information on possible sources, distances of transport, and depositional environments of the gold and other heavy minerals (Knight et al. 1999; Youngson and Craw 1999; Townley et al. 2003; McClenaghan and Cabri 2011; McClenaghan and Paulen 2018; Nikiforova 2021; Chapman et al. 2021, 2022a,b). The study of these features contributes to understanding of placer gold concentrations that have been mined extensively around the world (Boyle 1979; Henley and Adams 1979; Garnett and Bassett 2005). Gold compositions, particle morphologies, internal structures, and micro-inclusions are the principal features of detrital gold that contribute to understanding of the sources and transport pathways within a fluvial sedimentary system (Knight et al. 1999; Youngson and Craw 1999; Townley et al. 2003; Chapman et al. 2021, 2022a,b). Most such gold has developed deformed shapes after relatively short transport distances (km to tens of km; Youngson and Craw 1999; Knight et al. 1999; Townley et al. 2003; Chapman et al. 2022b; Masson et al. 2022). Eventually, flakes can have complex structure in detail, becoming folded and refolded and thinned with progressive transport (e.g. Figure 1a–d; Craw and Youngson 1999; Townley et al. 2003; McLachlan et al. 2018; Chapman et al. 2022b).

Morphology and structure of placer gold from young marine and marginal marine environments around the world have been less studied than from fluvial placers, partly because these placers have been less commonly mined and partly because the gold is especially finely particulate (Boyle 1979; Eyles 1990; Garnett 2000; Reznik and Fedorunchuk 2000; Garnett and Bassett 2005; Hou et al. 2017; Ritchie et al. 2019; Kungurova 2021). One of the few published depictions of detailed morphology of possible fine marginal

Editorial handling: A. R. Cabral

✉ Dave Craw
dave.craw@otago.ac.nz

[1] Geology Department, University of Otago, PO Box 56, Dunedin 9054, New Zealand

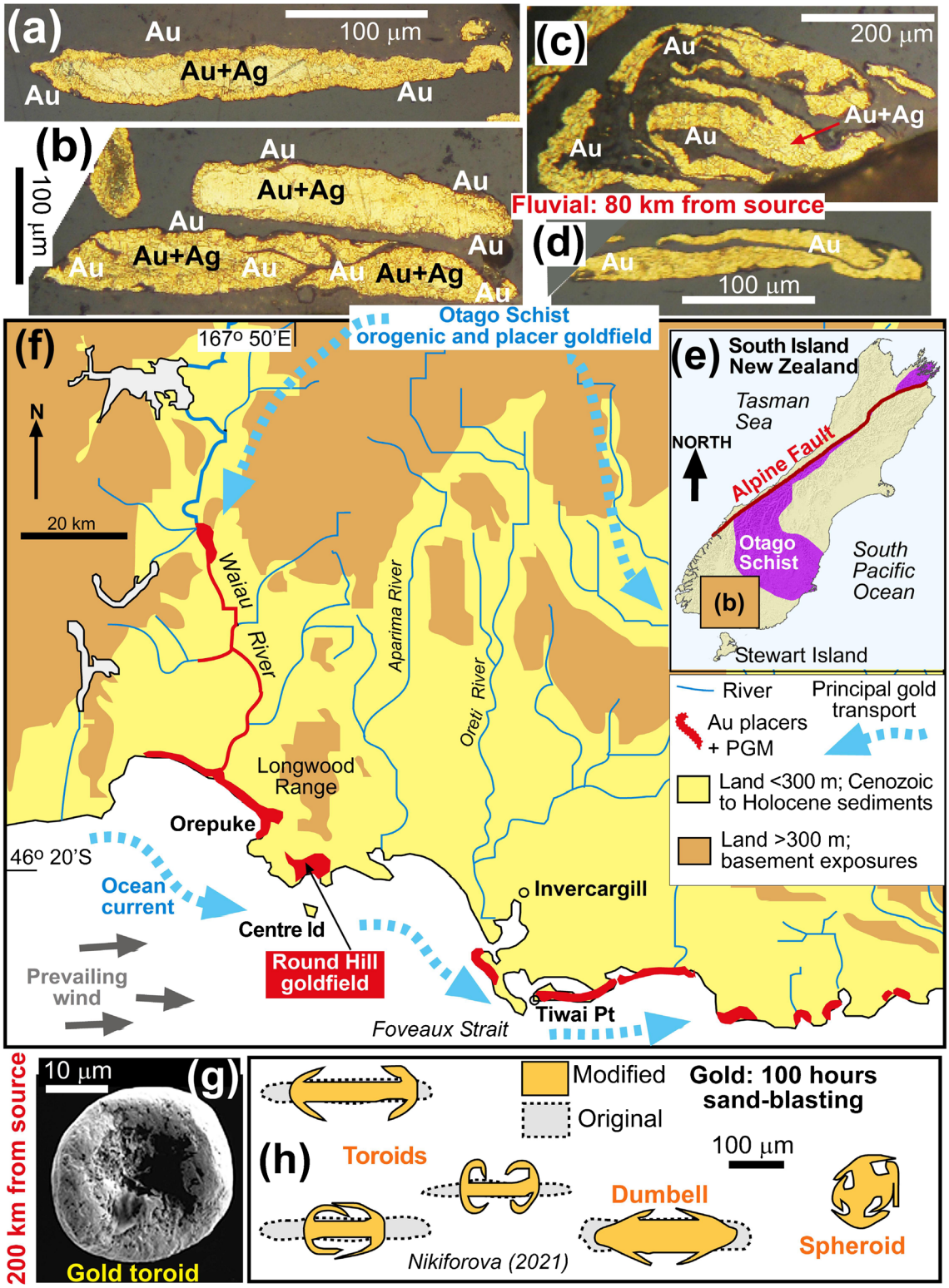

Fig. 1 Physical and geographic setting for this study of gold particle transformation processes and the gold textures produced. **a**–**d** Reflected light views (etched) of typical fluvial gold flakes after ~ 80 km of transport from Otago Schist (after McLachlan et al. 2018). Ag-bearing cores are surrounded by Ag-free gold rims, except for **d**. Flakes in **c** and **d** are folded. **e** Location map for study area in the South Island of New Zealand. **f** Summary topographic map of the coastal area for this study and its immediate hinterland, including source of placer gold in Otago Schist. PGM, platinum group minerals. **g** Typical toroid on modern beach in the area of this study. **h** Sketches of experimental transformations of detrital gold by aeolian sandblasting (modified from Nikiforova 2021)

marine gold was produced by X-ray imaging of fully lithified Archean ore (Holzing et al. 2015). Finely particulate gold in young sediments (herein called fine gold, typically ~ 100 µm or finer) is difficult to sample as it can float on water and/or can be carried off with other heavy minerals during concentration processes (Craw et al. 2013; 2015a; Shuster et al. 2016; Ritchie et al. 2019; Craw and Kerr 2021; Kungurova 2021). These sampling difficulties are particularly strong for toroidal and spheroidal beach gold that is generally compact and equant rather than flaky in shape (Guisti 1986; Craw et al. 2013, 2015a; Craw and Kerr 2021; Nikiforova 2021).

In this study, we extend recent research on the nature and context of aeolian toroid-bearing Pleistocene recent gold placers on the southern coast of New Zealand (Fig. 1e–g; Craw et al. 2013, 2015b; Craw and Kerr 2021). We document the morphology, internal structure, and chemistry of fine aeolian gold in order to infer some of the specific processes that lead to evolution from flaky fluvial gold (e.g. Figure 1a–d) to form toroids and spheroids in a marginal marine setting (e.g. Figure 1g,h). We focus on the fine gold particle fraction of a placer mine operation developed in Pleistocene marginal marine sediments near Round Hill (Fig. 1f). This site has provided a rare sampling opportunity as the processing system is tuned to save fine gold, whereas this fine gold fraction is commonly not saved or is poorly represented in field and laboratory sampling situations and in other mines elsewhere in the world (e.g. Kungurova 2021).

General setting

Gold in the placer in this study was derived ultimately from the Otago Schist orogenic and placer goldfield, ~ 200 km to the north (Fig. 1e,f) and underwent several stages of recycling and downstream transport over that 200 km throughout the Cenozoic (Upton and Craw 2016; McLachlan et al. 2018; Craw and Kerr 2021; Chapman et al. 2022b). Gold particle transport and associated recycling in that complex history resulted in strongly deformed and folded flakes, as observed at intermediate stages in that pathway (Fig. 1a–d). The sources of coexisting platinum minerals in the placers are not well defined, but most are inferred to have been derived from an ophiolite belt on the southwestern margin of the Otago Schist (Fig. 1e,f) and undergone similar fluvial transport to the gold (Craw et al. 2013). Some more locally derived platinum is inferred to have come from gabbro in the Longwood Range that forms the basement to this study area (Fig. 1f; Ashley et al. 2012; Craw et al. 2013).

The coastal placer system has been fed by the Waiau River catchment since the Miocene (Fig. 1f; Upton and Craw 2016). However, during times of lower sea levels, the area that is now offshore was a broad flat fluvial plain (Cullen 1967), and heavy minerals were transported farther south. The currently observable beach placers were formed at times of relatively high sea level, as at present. The coastline is undergoing slow tectonic uplift, and placer-bearing Pleistocene beaches > 200 ka are preserved ~ 50 m above present sea level (Turnbull and Allibone 2003; Craw et al. 2013; Craw and Kerr 2021). The best developed concentrations of heavy minerals, including most of the mined gold and platinum, occur where uplifted Pleistocene beaches have been eroded into short streams that recycled these beach sediments back towards the coast (Turnbull and Allibone 2003; Craw and Kerr 2021). Gold and platinum minerals have accumulated principally at the base of these short paleochannels, especially where they were incised into the basement (Craw and Kerr 2021).

The coastline in this area is exposed to strong winds and associated surface currents directed onshore from the west and southwest, in the global-scale wind system known colloquially as the Roaring Forties (Figs. 1f and 2a–d). The winds and currents drive strong surf on to beaches, with a general longshore drift of sediments from west to east (Figs. 1f, 2a,b and 3a). Active beaches are washed by strong surf on a daily basis, forming localised concentrations of heavy minerals, including gold and platinum minerals (Fig. 3a). Prevailing winds from the west that sweep around the coast commonly gust over 50 km/hour and periodically exceed 100 km/hour (Fig. 2c,d). These winds regularly drive sand at high velocities across beaches, to pile up as dunes on low-relief landward areas (Fig. 2b). The wind systems are likely to have been similar or stronger at times in the Pleistocene (Crundwell et al. 2008). Extreme Pleistocene wind-blown sand erosion on the exposed west coast of nearby Stewart Island (Fig. 1e) has formed granite ventifact cobbles and associated wind-sculpted granite outcrop surfaces (Bishop and Mildenhall 1994).

Sample site and methods

Material for this study was obtained from a mining company with an active placer mine in a Pleistocene paleochannel draining from the Longwood Range (Fig. 2b; Craw and Kerr 2021). The mine is a small–medium-sized operation which produces between 500 and 1000 oz (15–30 kg) of gold per year. The hosting paleochannel is the Pleistocene course of the modern Ourawera Stream (Fig. 2b) and contains recycled and reconcentrated heavy minerals from raised beach sand concentrates on the lower slopes of the Longwood Range (Fig. 2b). These natural concentrates are dominated by garnet and ilmenite (Fig. 3a,b). Gold, with minor platinum, was mined historically in the headwaters of this paleochannel, and a modern mine was developed in the middle reaches (Fig. 2b). The paleochannel is covered by thin (~ 20 m) Pleistocene–Holocene terrestrial and marginal marine sands,

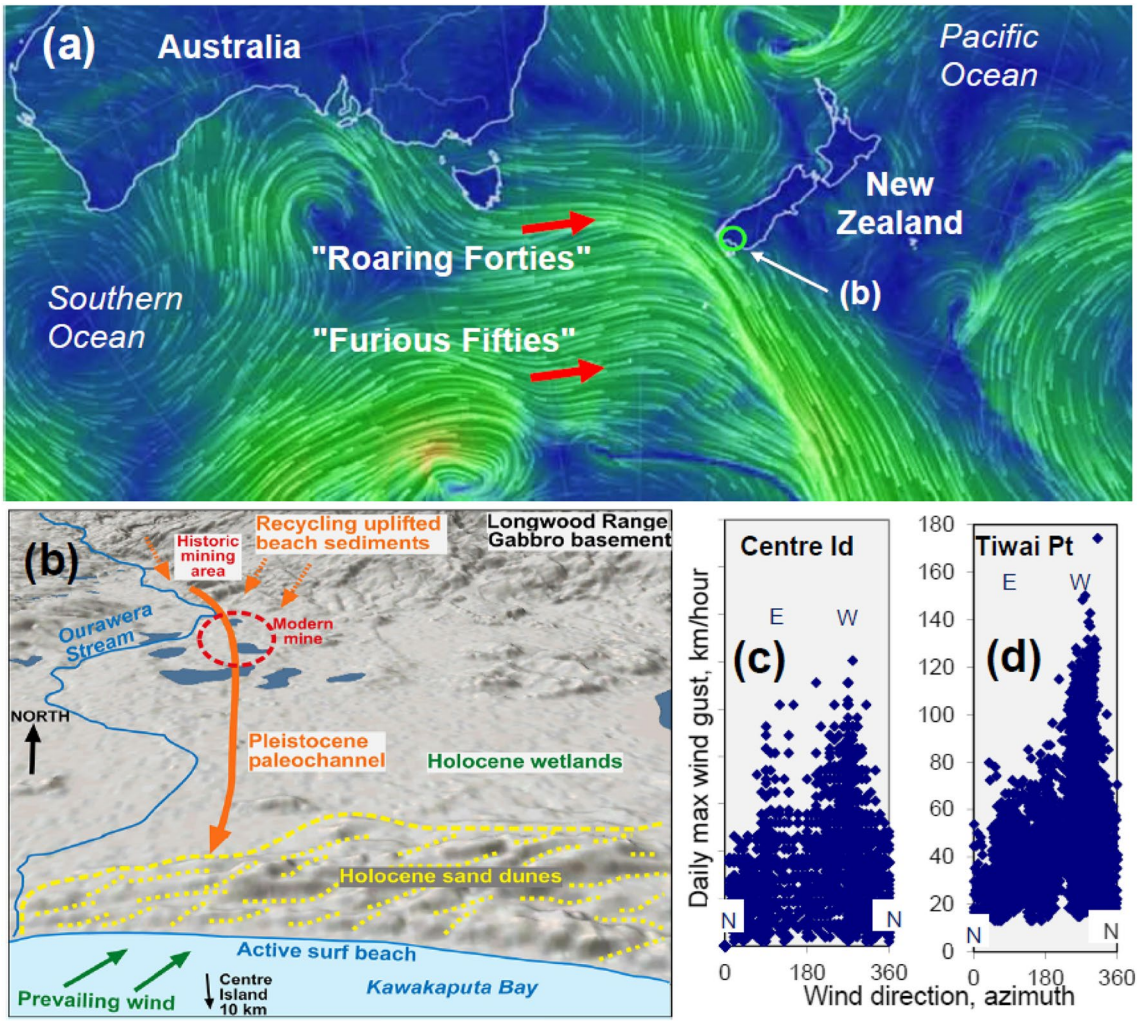

Fig. 2 Physical setting for the marginal marine site of this study. **a** Typical wind patterns in the Southern Ocean (from earth.nullschool.net) that lead to prevailing west to southwest winds in southern New Zealand. **b** Oblique DEM looking north from the south coast to the Round Hill mining area (Fig. 1f), showing location of mined Pleistocene channel that underlies the Holocene surficial deposits. The mine is 3 km from present coast. **c**,**d** Representative data for maximum daily wind gusts (from cliflo.com.nz; same scales for both) at weather stations in the vicinity of the study area (located in Fig. 1f)

silts and muds, organic-rich wetland sediments, and Holocene beach-margin sand dunes in the lower reaches (Fig. 2b).

The studied heavy mineral concentrate (Fig. 3c–f) was obtained from the end of the routine production-processing stream. Several stages of gravity settling of heavy minerals from an ore slurry initially yielded a mine concentrate rich in gold and platinum minerals. Relatively coarser gold (~0.5 mm) was removed from this mine concentrate by mercury amalgamation, but this process did not affect the fine gold fraction or the platinum (Fig. 3d–f). The resultant residual tailings from the amalgamation stage contained relatively abundant fine toroidal gold particles, which are generally difficult to save during commercial extraction or recreational panning. The sample examined in this study included > 1000 flakes of a mixture of gold and platinum (Fig. 3c–f), including several hundred toroidal particles.

Initial observations of exterior surfaces of particles in the sampled material were made via standard light stereomicroscopy. Subsets of particles were mounted onto aluminium stubs using double-sided carbon tape for more detailed observations on particle morphology on a Zeiss Sigma VP (variable pressure) scanning electron microscope (SEM) at the Otago Micro and Nanoscale Imaging (OMNI) (University of Otago, New Zealand). Backscatter electron images (BEI) were obtained at 15 kV without carbon coating. Identifications and compositions of heavy mineral particles, including platinum minerals, were obtained using energy dispersion analytical facility (EDX) on the SEM.

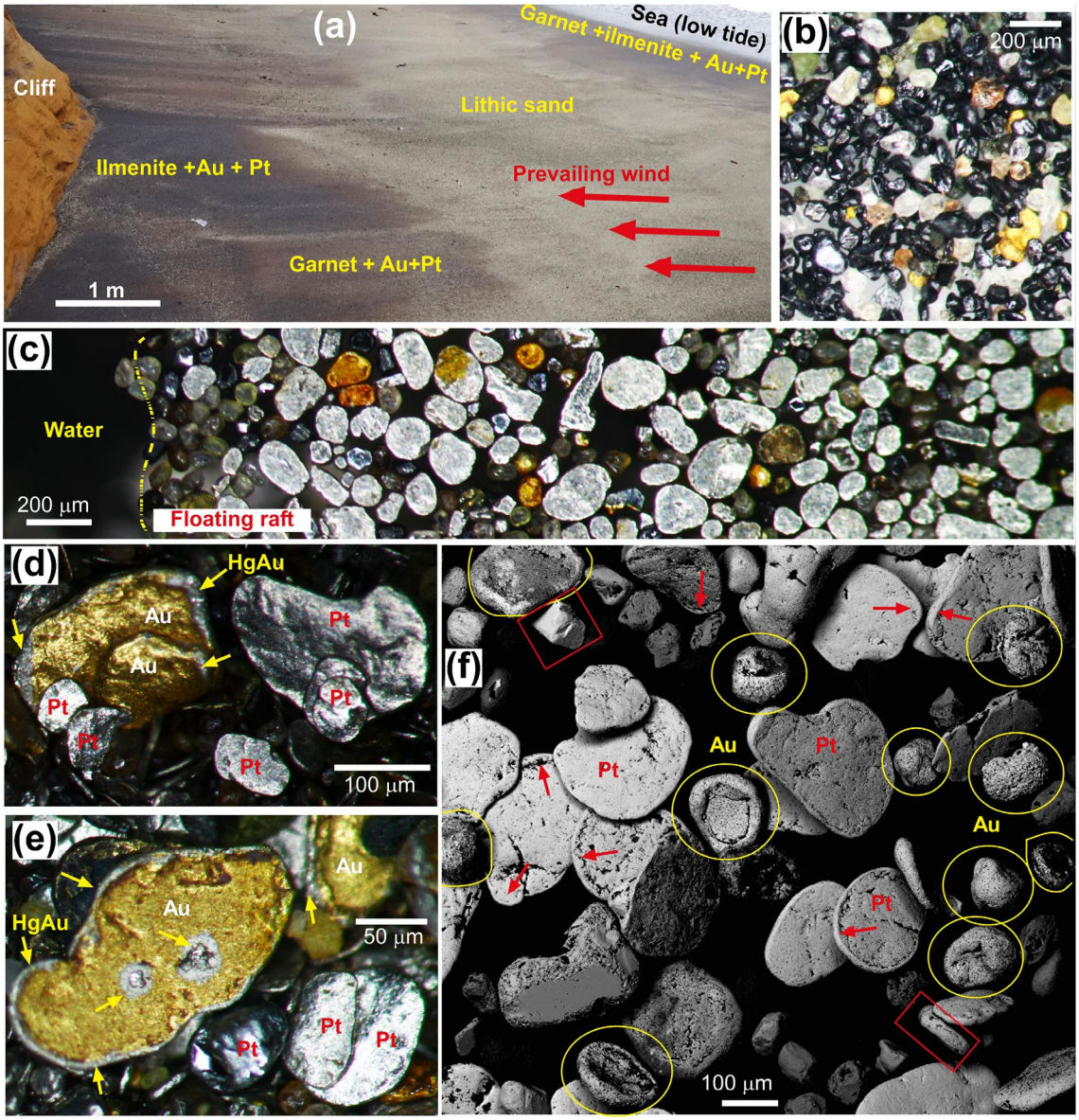

Fig. 3 General mineralogical setting for the mine concentrate examined in this study after passing the Hg amalgamation stage. **a** Modern beach (Orepuke, Fig. 1f) with heavy mineral concentrates (including gold and Pt minerals) formed naturally by surf and exposed to wind abrasion at low tide. **b** Heavy mineral concentrate from the modern Round Hill mine: black = ilmenite and magnetite; red and pink = garnet; green = epidote and apatite; yellow = gold; white = zircon. **c** Gold (yellow) and platinum (white) flakes in production concentrate from the modern mine, after Hg-amalgamation, photographed forming a floating raft on water surface despite much agitation. **d**, **e** Gold and platinum mineral flakes in production concentrate. Coarser gold has been removed as Hg-amalgam, leaving finer gold, some of which has minor Hg-amalgam (yellow arrows). **f** SEM backscatter image of production concentrate after amalgamation (as in **c**,**d**,**e**). Gold toroids are in yellow circles. Some ferroan platinum flakes have incipient toroidal rims (red arrows). Euhedral platinum mineral particles are indicated in red squares

Random selections of particles were shaken on to sticky tape before being embedded in 25-mm epoxy resin discs that were then ground to expose sections through the particles. These two-dimensional sections lack a third dimensional view, but the sheer abundance of particles available in the mine production concentrate largely compensates for this two-dimensional bias. The discs were finely polished with a 1-µm diamond paste for examination initially via reflected light microscopy. The discs were then etched with *aqua regia* to remove the smeared surficial gold polishing layer, and then coated with a 10 nm thick layer of carbon (Stewart et al. 2017). Etching of gold containing silver (Ag) commonly leaves an irregularly distributed

Ag-bearing surficial residue that interferes with EDX analysis, making such analyses semi-quantitative only.

Internal grain structures of etched gold particles were revealed by electron backscatter diffraction (EBSD) maps that were generated using the same Zeiss VP FEG SEM equipped with an Oxford Instruments Nordlys F EBSD camera (Prior et al. 1999, 2009; Stewart et al. 2017; McLachlan et al. 2018). The EBSD patterns were collected in high vacuum mode with the sample tilted to 70° and using an accelerating voltage of 20 kV, aperture of 300 µm and a working distance of ~ 30 mm. The gold particles were mapped by scanning the electron beam over rectangular map areas that were of the order of 100 µm wide and 100 µm high using a step size of 0.3, 0.4, or 0.5 µm. The EBSD patterns were illuminated on a phosphor screen and imaged by the EBSD camera using the Speed 2 Binning Mode, an exposure time of 1.75 ms and camera gain of 1. The imaged EBSD patterns were automatically indexed by Oxford Instruments Aztec version 4.1 SP1 software, and the resulting EBSD data was exported to HKL Channel 5 for cleaning and processing. Maps were cleaned using the noise reduction module, which started with removal of 'Wild spikes' and was followed by iterative replacement of zero solutions that have down to 6 similar neighbours. EBSD map pixels were digitally coloured according to crystallographic Euler angles (Nolze 2015), using the Aztec software, and are presented as inverse pole figure (IPF-X) maps. Crystallographic misorientation maps were created in which pixels were coloured according to average local misorientations below the subgrain angle of 2° using a rectangular filter size of 3 × 3. Grain boundaries were added where misorientation angles were > 10° and sub-grain boundaries were added where misorientation angles were > 2°. Etching with *aqua regia* tends to enhance dissolution of grain boundaries and other discontinuities such as polishing scratches, and that enhanced dissolution results in sloping surfaces at the micron scale that are not easily indexed by the EBSD system, leaving blank pixels in some areas. Attempts at producing EBSD maps of platinum particles accompanying the fine gold had only limited success (on euhedral particles), and this was not pursued on platinum flakes.

Terminology

There can be terminological confusion whereby the same words are used for different meanings in studies such as this one in comparison to other published works, so we define here our usage of words (as initiated in above text) that are most likely to cause confusion. *Particles* are detrital mineral fragments that have undergone sedimentary transport. Most of these *particles* have internal structures made up of interlocking mineral *grains* that have various crystallographic orientations. *Fine* (and *coarse*) particles refer to the overall size of the particles, in contrast to *grain size*, which is an internal feature of the particles and is commonly variable within particles. *Gold* is an Au–Ag alloy, typically a particle, and we refer to compositions of that alloy in general terms of whether it is *Ag-bearing* or *Ag-free*, labelled in particle interiors in several figures herein as *Au* + *Ag* and *Au*, respectively. In the context of EDX analyses as outlined above and our previous work (e.g.Craw et al. 2013; McLachlan et al. 2018), this distinction is equivalent to 1–10 wt% Ag for Ag-bearing gold and < 1 wt% for Ag-free gold. Consequently, we specifically avoid referring to gold compositions in terms of fineness (cf Craw et al. 2013). Some artificial (process-related) amalgams of gold and mercury are depicted as *HgAu*.

Results

Gold morphology and composition

Gold particles show a range of external shapes, from toroidal flakes to spheroids (Fig. 3c,f and 4a–g). The most distinctive features of many of the flaky gold particles are their thin attenuated margins that have curled around the edges of the particles (Figs. 3c,f and 4a–g). These attenuated margins form the toroidal rims and extend towards the centres of the particles (Figs. 4a–g and 5a–i). Some of these attenuated edges have become so extended that they overlap in the particle centres (Fig. 5f–i). A combination of this extension of margins and overall shortening of the flake centre has led to formation of spheroids with complex internal structures (Figs. 4e–g and 5d,g–i). Some of the spheroids have been formed from thinly extended toroidal flakes that have been refolded in on themselves (Fig. 5g–i). These, and other similar spheroidal particles, have multiple internal strands (5 g–i). All toroids and spheroids observed in this study have at least some clay adhering to exterior and interior surfaces (Fig. 4a–g), although most clay was washed from the particles in Fig. 5a–i during sample preparation.

Portions of the cores of many toroidal flakes have remnants of Ag-bearing gold (Fig. 5b–g) that formed the core of most original fluvial flakes (e.g., Fig. 1a–c). Likewise, some of the larger internal strands of more complex particles have remnants of this Ag-bearing gold. These contrasting gold compositions are difficult to resolve with SEM–EDX analysis because the boundaries between areas of different composition are complex and interdigitated at the 3-µm scale of the electron beam. However, the differential etching and contrasting colours of electron backscatter images suggest that the boundaries are sharp at the micron scale (Fig. 5b–d). The central portion of the spheroid in Fig. 5d has 14–16 wt% Ag.

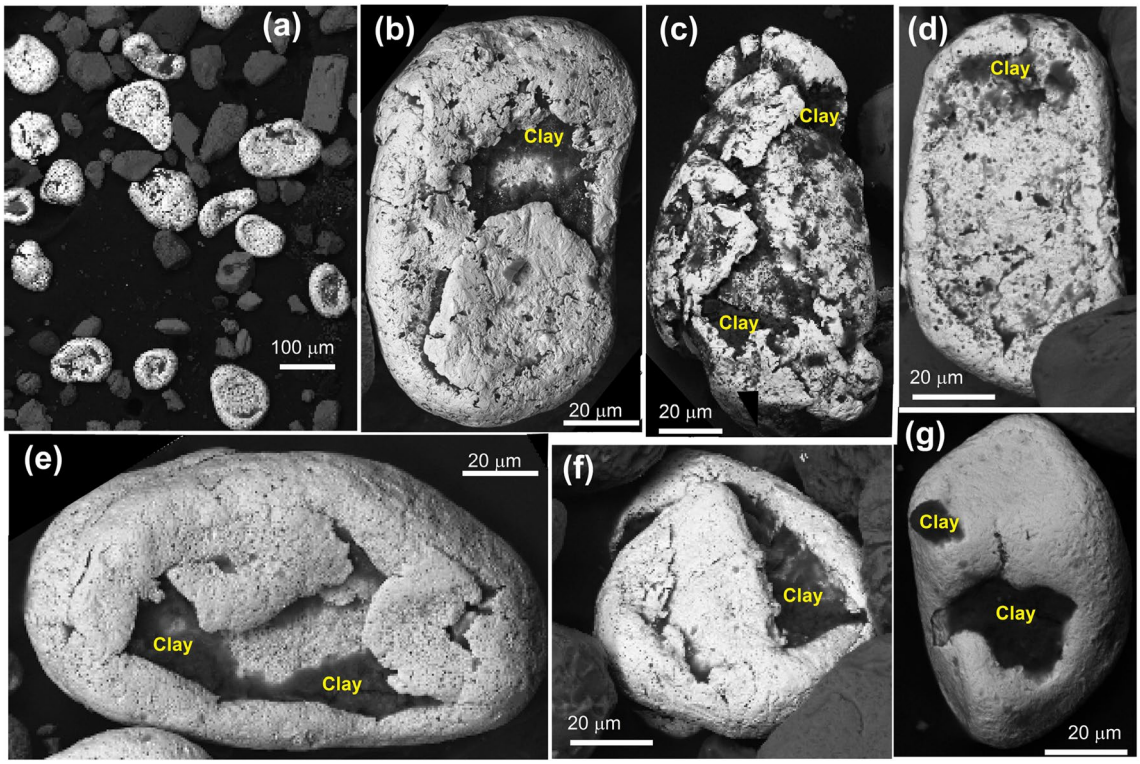

Fig. 4 SEM backscatter images of gold concentrated from the modern mine, showing morphology of exterior surfaces and internal clay inclusions. **a** General view of gold particles. **b–d** Particles with complex thickened toroidal rims on flakes and extended protrusions. **e**,**f** Spheroidal shapes formed by extreme extension and folding of toroidal protrusions. **g** Spheroidal shape inferred to result from advanced toroidal development

Gold internal grain structure

The internal grain structure of the gold as revealed by EBSD analysis shows that there is a combination of relatively coarse grains and finer grains within each particle (Fig. 6a–f). The coarser grains are typically 10–20 µm across, whereas the finer grains are < 1 to 10 µm across, and different portions of each particle have clusters of these contrasting grain sizes (Fig. 6a–f). The coarser grains have apparently been partially replaced by clusters of finer grains in many parts of the particles. In the incipiently formed toroidal flake in Fig. 6a, coarse grains occur right around the exterior surface and extend into the attenuated margins, while the bulk of the particle consists of finer grains. Well-developed toroidal flakes have coarser grains in their interior portions and some minor patches of coarse grains elsewhere in the particles (Figs. 6a–e and 7a). Fine grains predominate elsewhere in the toroidal particles, especially in the attenuated edges (Figs. 6a–d and 7b–i). Some of the finest grains are undistorted (Fig. 7d,i), but many show some distortion (Fig. 7f,g).

The spheroidal particle in Figs. 5d and 6e has a distinct relict Ag-bearing core zone that consists of relatively coarse grains surrounded by finer grains that extend throughout the complexly attenuated margins. The coarse Ag-bearing grains have internal misorientations and have highly irregular edges where clusters of finer grains have partially overprinted these edges (Fig. 6e,f). Similar irregular edges and deformation microstructures are also evident in some of the coarse grains in other toroids (Fig. 6c,d). In contrast, the spheroidal particle in Figs. 6b and 7a has coarsest grains with variable misorientations on parts of the outer edge and finer grains with fewer misorientations in the central strand (Fig. 7b–i).

Platinum mineral morphology

Platinum minerals are not a principal topic of this study, as they were described in detail previously (Craw et al. 2013). However, the presence of platinum minerals, dominated by ferroan native platinum, with the toroidal gold in the mine concentrate presents a useful opportunity for direct comparison of the relative malleability of gold and platinum minerals in this setting. Platinum minerals occur as locally derived euhedral particles (Figs. 3f and 8a–c) and flakes that have undergone long-distance transport (Figs. 3f and 8d–g). Euhedral particles have textures indicative of only minor deformation during transport, such as fractured corners and/or incipient rounding (Fig. 8a,b). Internally, particle

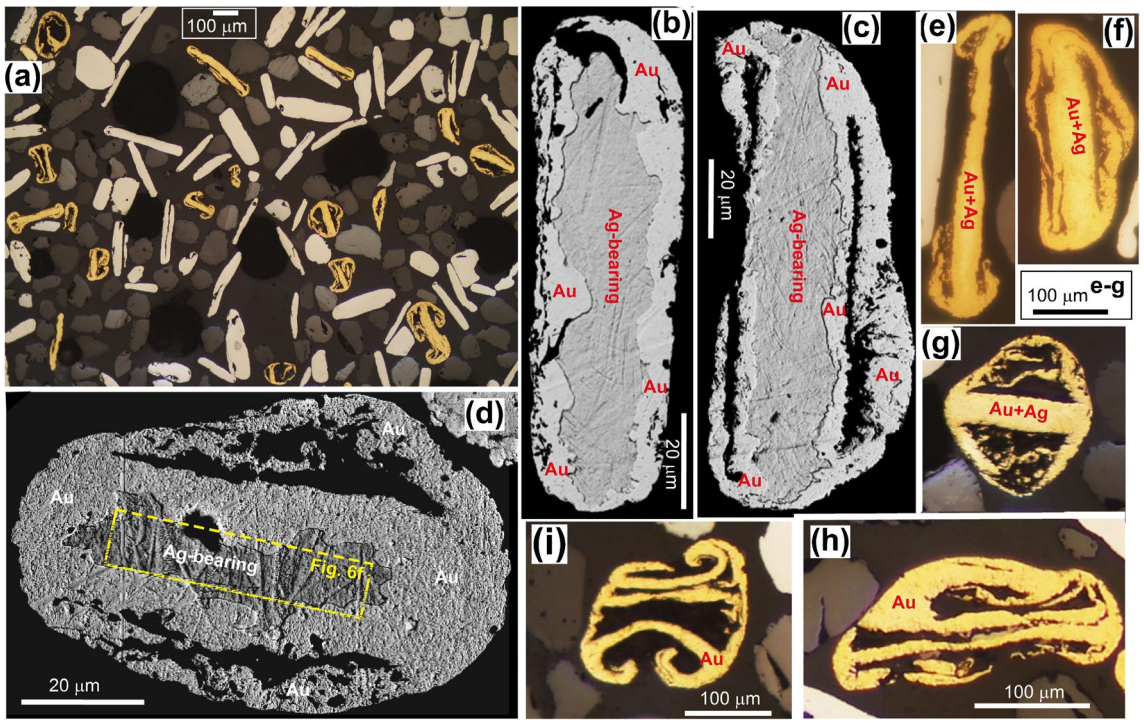

Fig. 5 Internal views of gold in production concentrate that passed through Hg amalgamation. **a** Reflected light view of concentrate, with ferroan platinum (white) and abundant gold toroid sections. **b–d** SEM backscatter images of gold toroids (**b**,**c**) and a spheroid (**d**) after *aqua regia* etching, showing Ag-bearing cores (darker) and Ag-free rims and folded toroidal protrusions (lighter). **e–i** Close reflected-light views of sections through toroidal and spheroidal gold, showing a progression in complexity from simple proto-toroidal flakes with Ag-bearing cores (e–g; paler colour in Ag-bearing centres, labelled Au + Ag) to multilayered forms that have uniformly low Ag (**h**,**i**)

rims show misorientations and some sub-grain formation accompanying external rounding (Fig. 8c,d). Particles that underwent long-distance transport are thin discoid flakes with rounded rims (Figs. 3f and 8e–h). There has been minor deformation of some of these rims to form incipient toroidal protrusions at the 10-µm scale (Figs. 3f and 8b,e–h). The scale of these toroidal protrusions is very small compared to the coexisting gold (Figs. 3f and 8g,h), and any larger-scale internal deformation in platinum minerals (e.g., Fig. 8c,d) is presumed to be a result of fluvial transport, not aeolian processes.

Discussion

Low-temperature gold transformations

Gold on the beaches of this study area (e.g. Figures 1g and 3a) arrives after a long-distance fluvial transport and associated deformation (Figs. 1a–d and 9a–d). The beach gold is then subjected to sandblasting whenever it is exposed and concentrated at the beach surface by surf action (Fig. 3a). The toroidal gold examined in this study formed initially on a Pleistocene beach under similar windy sandblasting conditions, or perhaps even windier conditions. The gold was subsequently uplifted, recycled a short distance downstream (1–2 km), and buried ~ 20 m deep in a paleochannel (Fig. 2b). Hence, all processes, fluvial and coastal, involved in these transformations of the gold morphology have occurred at low temperatures near to the present surface mean annual temperature of ~ 10 °C.

Despite the low temperature of these morphological transformations, there have been major crystallographic changes within the particles during fluvial transport and on beaches, of the types summarised in Fig. 9a–h. These transformations have been accompanied by the loss of Ag from the original Au–Ag alloys (Fig. 5b–i). Features in the transition from coarse-grained and variably deformed Ag-bearing gold to fine-grained and locally unstrained Ag-free gold are depicted in Figs. 6 and 7. However, the proportion of fluvial and aeolian contributions to these changes is not clear and is discussed in the next section.

This transition reflects progressive recrystallisation and annealing of the gold, similar to processes that occur in many other geological materials, typically at higher temperatures (Doherty et al. 1997; Prior et al. 1999, 2009). Deformation has led to crystallographic distortion and local sub-grain development in the coarse grains, as in Fig. 6e,f.

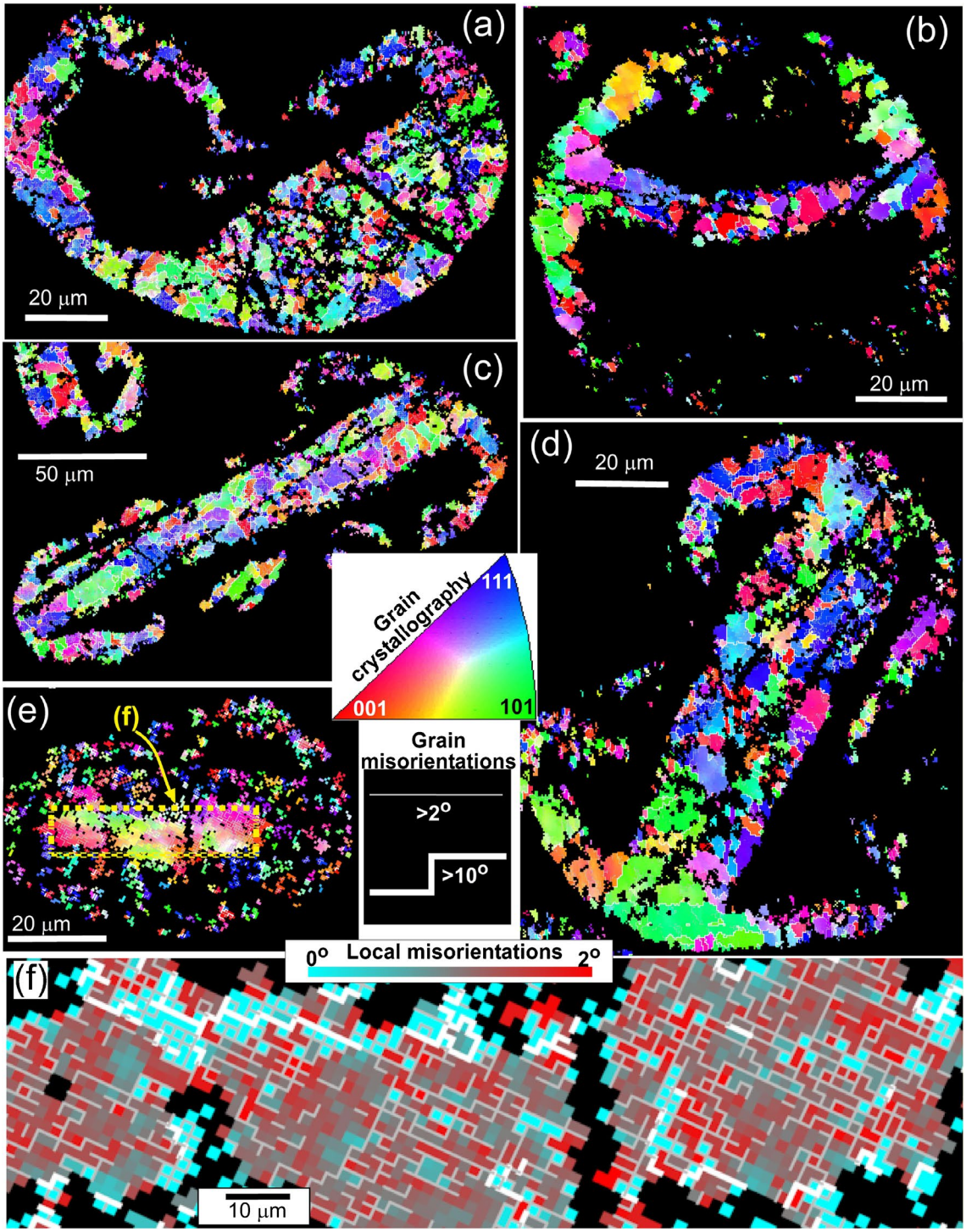

Fig. 6 EBSD maps of toroidal and spheroidal gold particles, showing internal grain sizes and structure. Grain misorientation boundaries at > 2° (thin grey lines) and > 10° (thick white lines) have been inserted. Stereographic triangle (centre) applies to IPF maps. **a** IPF-X map of deformed flake with attenuated proto-toroidal extremities. **b** IPF-X map of spheroidal particle (as in Fig. 7a–d). **c**,**d** IPF-X map of multilayered toroidal flakes. **e** IPF-X map of spheroidal particle in Fig. 5d, with thick coarse-grained Ag-bearing central strand. **f** Local misorientation map of coarse central grains in **e**, showing abundant internal misorientations

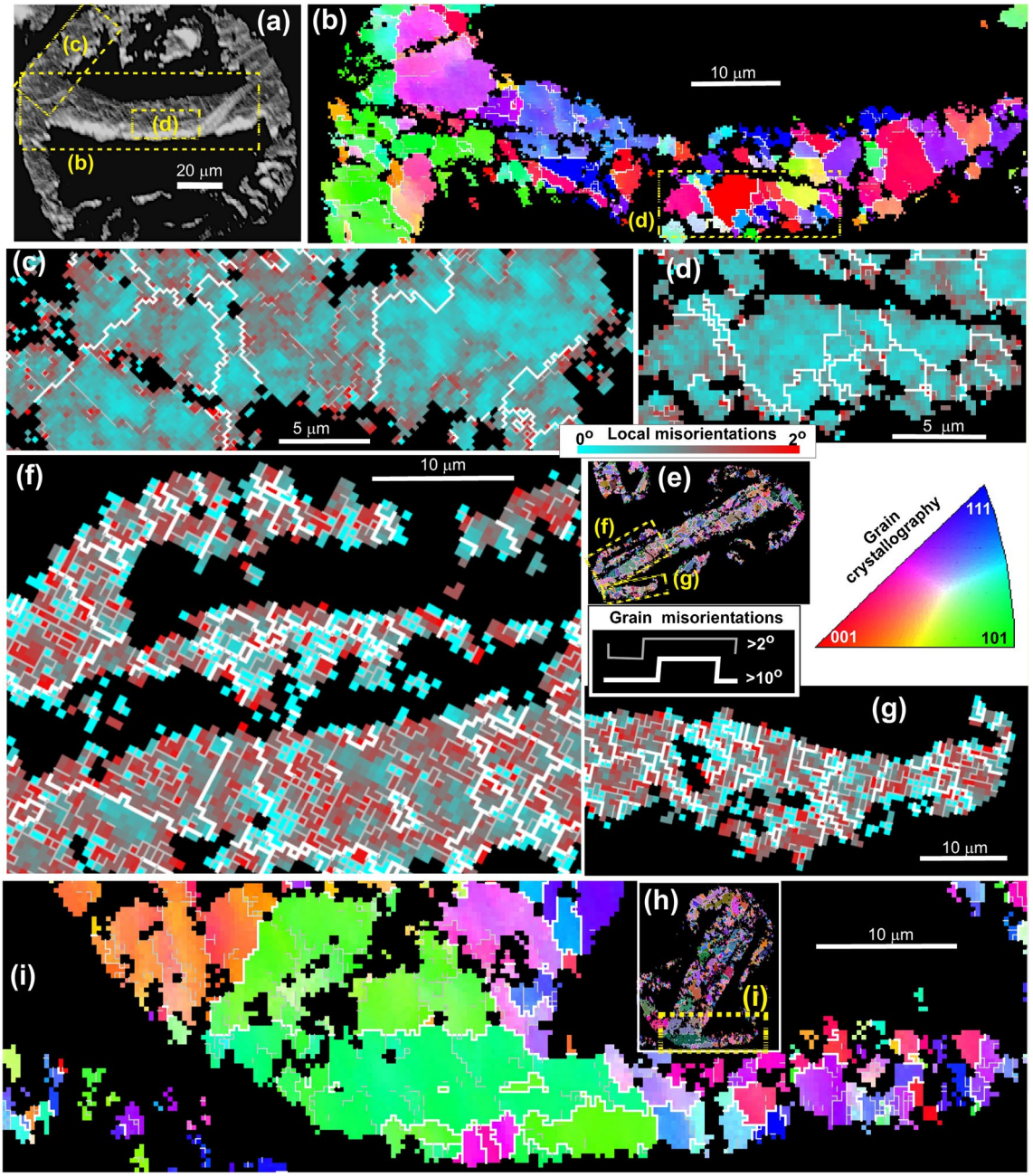

Fig. 7 Close views of EBSD maps (legends at centre right, as in Fig. 6), with associated index images to show locations. **a** BSE image of a spheroidal particle (as in Fig. 6b) with locations of maps in panels **b**–**d**. **b** IPF-X map showing contrasting grain sizes from outer edge (left) to central strand (right) of spheroid in **a**. **c** Local misorientation map of coarse grains on the outer edge of spheroid in **a**. **d** Local misorientation map of fine grains on the central strand of spheroid in **a**. **e** Toroid (Euler colours) showing locations of maps in panels **f** and **g**. **f** Local misorientation map of central strand and attenuated protrusions of toroid in **e**. **g** Local misorientation map of attenuated toroidal protrusion. **h** Toroid (Euler colours) showing location of IPF map in panel **i**. IPF-X map of fine grained toroidal protrusion (right) extending from coarse grained central strand (left)

The proportion of fine grains increased with increasing particle deformation, and micron-scale annealed grains became progressively more abundant, although many finer grains have subsequently been deformed as well (Fig. 7f,g). Fully annealed gold consists of interlocking fine grains with widely ranging crystallographic orientations and only minor distortion on outer grains (Fig. 7b,d).

Recrystallisation to relieve internal grain deformation as a result of cold-rolling of impure gold has been observed in industry-related experiments (e.g. Cho et al.

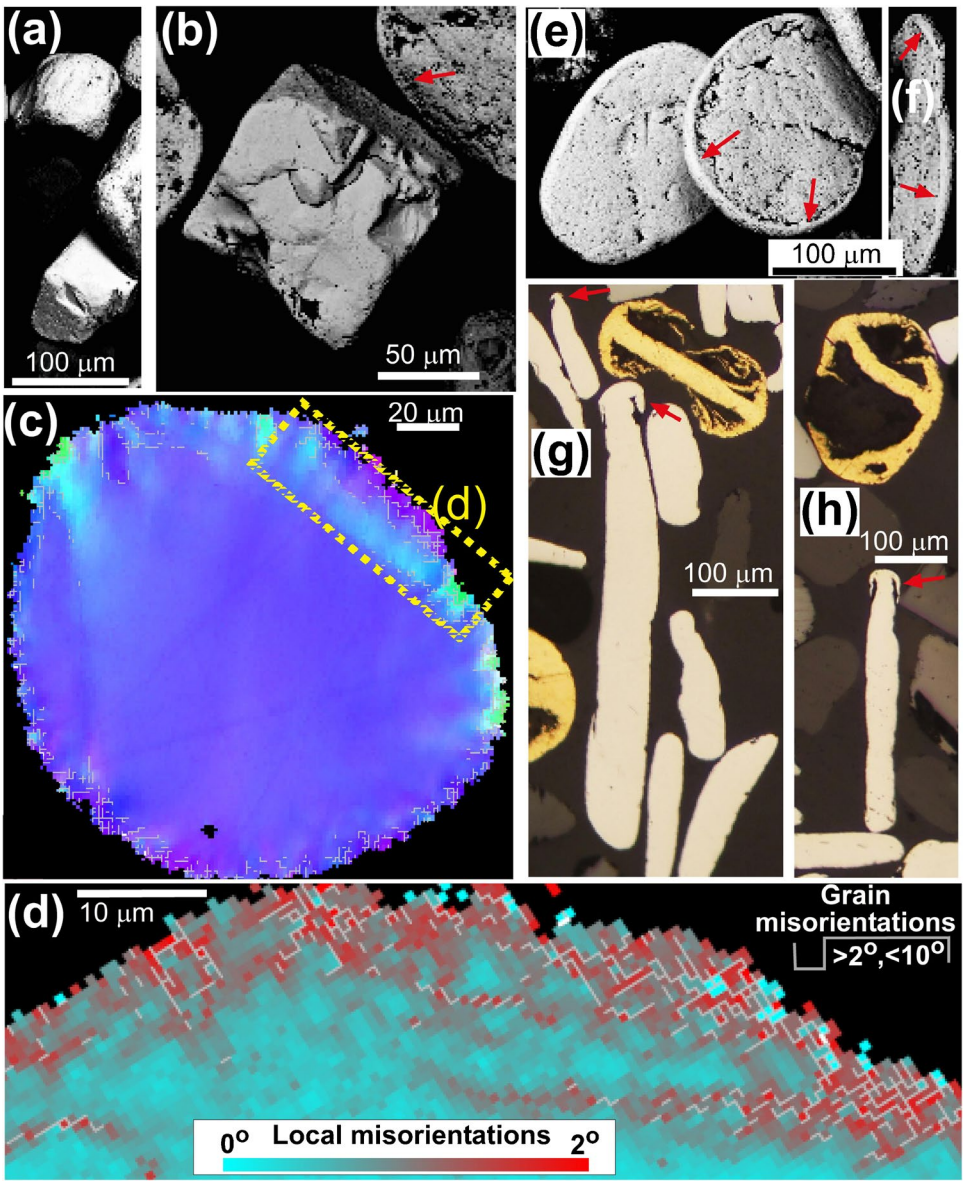

Fig. 8 Contrasting textures of equant and flaky ferroan platinum particles. Proto-toroidal rims are indicated with red arrows. **a**, **b** SEM backscatter images of angular and slightly rounded equant particles. **c** EBSD IPF map of a section through a rounded equant particle. Stereographic triangle as in Figs. 6 and 7 legends. **d** Close view of the rim of particle in **c**, showing abundant misorientations > 2° but < 10° on a local misorientation map. **e**, **f** SEM backscatter images of flakes with proto-toroidal rims, with flat face view in **d** and side-view in **e**. **g**, **h** Incident light views of sections through flakes with proto-toroidal rims indicated. Gold toroids are included for comparison

2005; Hui et al. 2018), but these experiments involved short-term (hours–days) annealing at elevated temperatures. Preferential removal of Ag to leave purer gold (dealloying) has also been studied in industry-related contexts (e.g.Erlebacher et al. 2001; Chen-Wiegart et al. 2013; Hui et al. 2018), although the specific aim of these experiments has been to produce nanoporous gold rather than the fully recrystallised gold observed in toroids. Our observations of the internal structure of beach gold (Figs. 6 and 7) suggest that similar processes to those that have been investigated on human time scales have occurred within the beach gold as a result of deformation under surficial low-temperature conditions.

Evolution from fluvial gold to aeolian beach gold

Morphological evolution of detrital gold in a river system principally involved development of flakes of decreasing thickness and increasing complexity (Figs. 1a–d and 9a; Knight et al. 1999; Youngson and Craw 1999; Townley et al. 2003; Chapman et al. 2022b). Most rims have recrystallised to low-Ag gold with grain size of typically 5–10 µm (Fig. 9b). More rarely, very fine-grained (locally sub-micron) surface smears have been imposed during fluvial transport (Fig. 9c,d; Kerr et al. 2017). The thin flaky fluvial gold has been the precursor for the beach gold that is mined at the site in this study, and some such flakes have survived despite

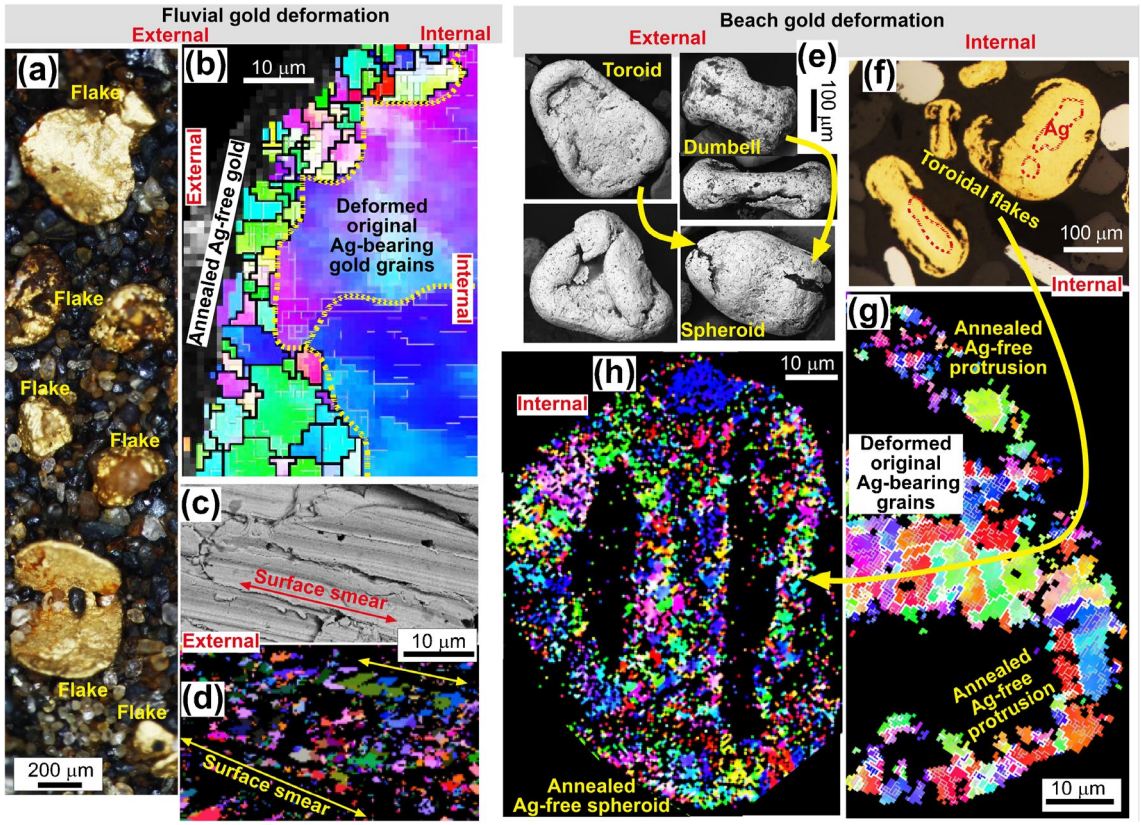

Fig. 9 Summary comparison of gold particle deformation between fluvially transported flakes (left, as in Fig. 1a–d) and beach gold in this study (centre and right). **a** External view of typical fluvial flakes. **b** EBSD IPF map of part of a section through a flake (after McLachlan et al. 2018) between fine-grained recrystallised Ag-poor rim (left) on coarse-grained deformed Ag-bearing core (right). **c** SEM backscatter image of a smeared mylonitic external surface (after Kerr et al. 2017). **d** EBSD Euler map showing fine grain size of smeared surface, as in **c**. **e** SEM backscatter images of beach gold (after Craw and Kerr 2021) showing external features in transition from toroidal flakes and dumbells to spheroids. **f** Incident light view of sections through toroidal flakes. **g** EBSD IPF map of the rim of a toroidal flake with relict coarse-grained Ag-bearing gold (centre left) and protrusions of finer grained Ag-poor gold. **h** EBSD IPF map of a section through a fully recrystallised fine-grained Ag-free spheroid

the aeolian beach processes (Craw et al. 2013, 2015a; Craw and Kerr 2021). These flakes have been mostly removed by Hg amalgamation from the concentrate used in this study (remnants in Fig. 3d,e).

The fine aeolian gold that has persisted through Hg amalgamation to occur in the amalgamation tailings that constitute the studied material has more compact and complex morphology than fluvial flakes (Figs. 4a–g and 5a). Experimental work by Nikiforova (2021) has shown that only 100 h of sandblasting is needed to produce toroidal and spheroidal particle shapes (Fig. 1h), and in the real beach environment, intermittent sandblasting occurs on time scales of weeks to years (Figs. 2b–d and 3a). Hence, we infer that aeolian beach processes have physically transformed the shapes of the particles described in this study. The resultant cumulative lateral extent of thin elongated strands within a complex aeolian particle such as that depicted in Fig. 5h is > 1 mm and is therefore broadly similar to highly deformed fluvial flakes, such as those in Fig. 1c,d, that are plausible precursors.

The coarse grains in both fluvial flakes and aeolian gold are probably primary features inherited from the source gold deposit (Stewart et al. 2017; Chapman et al. 2022b). Strain effects seen in the coarse grains in aeolian beach gold may have been inherited from the fluvial stages of transport, or imposed by sandblasting on a beach, or resulted from a combination of both sources of deformation. In this context, some multiple strands in the cores of the aeolian beach gold (e.g., Fig. 5g–i) may have been inherited from folded fluvial flakes (e.g., Fig. 1c,d) with inherited coarse grains that may have been already been strained (e.g., Fig. 6b,c).

Similarly, at least some of the recrystallised fine grains in toroidal particles may have been inherited from the precursor fluvial flakes. However, the fine grains in the more extremely attenuated rims of toroidal and spheroidal gold (1–2 µm; Figs. 6a–e, 7d,f,g,i and 9g) are smaller than those typically found on the rims of fluvial gold (5–10 µm; Fig. 9b). The fine grains that form the attenuated margins of the aeolian beach gold more closely resemble the micron-scale grains

in smears on the margins of fluvial gold that have been derived via focused deformation of the Ag-free fine gold rims (Fig. 9d; Kerr et al. 2017). Hence, there is an apparent grain-size difference between fluvially generated fine, Ag-free gold, and fine gold generated by sandblasting.

We conclude from these observations that most of the fine grains in the highly attenuated and delicate protrusions that characterise some toroids and the spheroids (e.g. Figure 9h) were formed by deformation and recrystallisation during and after the sandblasting process, and these processes have overprinted many grain structures inherited from the fluvial regime. This wind-driven deformation and recrystallisation may also have spread towards the cores of the particles to deform and partially recrystallise the relict coarse grains (Fig. 6e,f), especially coarse grains that are close to the margins of the particles. These recrystallisation processes were accompanied by the loss of Ag, which was presumably leached along evolving grain boundaries in a similar manner to that inferred for fluvial gold transformations and Ag loss (Craw et al. 2017; Stewart et al. 2017). In the beach environment, this loss of Ag may have been facilitated by dissolution during twice-daily tidal inundation by chloride-rich seawater.

Economic implications

The only positive economic effect of the aeolian transformation processes of beach gold has been continued extraction of Ag from relict coarse grains, a process that is initiated in the fluvial system (Fig. 1a–d), and has some economic significance as the bulk gold produced by a mine is more pure (Craw et al. 2017). Apart from that point, the results of this study provide physical and mineralogical context for the well-known difficulties of concentrating and saving fine beach gold during mining (Kungurova 2021). These concentration issues are mostly described in unpublished company reports and folklore of recreational panners and have received little previous scientific study. The tendency of fine flaky minerals to float on the surface tension of water is a common phenomenon (e.g. platinum minerals in Fig. 3c). However, flotation of more equant, even spheroidal, beach gold observed in this study helps to explain why that gold is so elusive in concentration processes (Fig. 3c).

The issues of floating gold and entrainment with other heavy minerals are made even more problematic because the toroidal and spheroidal gold particles have high internal surface area in a compact morphology (Fig. 5a–i). That compact shape commonly includes air, water, or clay minerals (e.g. Figure 4b–g) that lower the average density of the particles. The small-size compact nature and lower net density of these aeolian gold particles mean that they are readily entrained with other more abundant heavy minerals, in this case garnet and ilmenite (Fig. 3a,b), and do not readily sink in a processing slurry. In addition, the small size and compact morphology of the fine beach gold, especially spheroids, helps to resist Hg amalgamation because the surface tension of spherical Hg droplets is too great to allow Hg interaction, compared to associated gold flakes that are more reactive (Fig. 3d,e). Clay coatings on parts of the exterior of particles (Fig. 4b–g) further inhibit Hg amalgamation by separating Hg droplets from the gold (Malloch et al. 2017).

Not all beach gold globally is toroidal, since abundant beach toroid formation requires a relatively rare setting and set of associated processes (Fig. 2a–d; 3a). However, incipient toroid formation can occur in less favourable beach settings (e.g. Craw et al. 2006) and contribute to gold concentration inefficiency. Conversely, toroids can occur in placer deposits far from the coast (Giusti 1986; Youngson 2005; Nikiforova et al. 2011) and thereby contribute to gold concentration inefficiency as well. As a result of all these features of fine aeolian gold, efficient extraction is extremely difficult and monitoring of that efficiency by, for example, panning gold mine tailings, is also difficult for the same reasons. Anecdotal evidence from the mine in this study indicates that repeated reprocessing of tailings always produces more fine gold, albeit uneconomically.

Conclusions

Toroidal and spheroidal gold particles with delicate, complex, and compact shapes were formed by sandblasting on active surf beaches on an exposed coast subjected to frequent strong winds. This aeolian gold was formed from thin flakes transported 200 km to the area by rivers. Fine aeolian gold particles (~ 100 µm) are difficult to concentrate and save in a mining environment because they commonly float on water, become entrained with more abundant heavy minerals, and resist amalgamation with Hg. These effects are exacerbated by the presence of clay within the particles, as the average density of particles is lower and clay inhibits surface interaction with Hg. This study focused on fine aeolian particles that bypassed Hg amalgamation in an active mine in Pleistocene marginal marine sediments.

Sandblasting has caused low-temperature deformation of the gold into the complex shapes. Edges of particles have become strongly attenuated to form multiple strands that are typically only ~ 20 µm across within particles, but have cumulative linear extents of ~ 1 mm, similar to the precursor fluvial flakes. Internally, some original coarse (> 40 µm) grains remain and these retain original Ag contents (1–10 wt%). These coarse grains show substantial internal crystallographic misorientation and sub-grain formation. Most of the gold in the attenuated margins has recrystallised to finer and less-deformed grains (1–2 µm) with little or no Ag (< 1 wt%). This recrystallisation was induced by the sandblasting

processes and subsequent annealing. The amount that aeolian-driven microstructural transformations extend into the core of the gold particles is not clear, as some strained grains and associated recrystallised grains may have been inherited from the fluvial stages of transport. However, coarse grains on the exterior of toroidal and spheroidal particles have almost certainly been partially recrystallised, with loss of Ag, by aeolian processes.

The high malleability of gold that has permitted formation of toroids and spheroids is strongly contrasted with the much harder platinum minerals that accompany the gold and have had a similar deformation history. Ferroan native platinum flakes have only incipient development of toroidal edges, at the 10-micron scale, and minor internal crystallographic deformation has been inherited from fluvial transportation.

Acknowledgements Access to the Round Hill mine was kindly facilitated by Ray Stewart and Mark Skinner, and their on-going discussions on the site were very helpful in developing this study. SEM work was conducted at the Otago Micro and Nanoscale Imaging (OMNI) facility, University of Otago, New Zealand. Gemma Kerr assisted with SEM imaging. Helpful review comments from Rob Chapman, Andre Barretto, an anonymous referee, and Associate Editor Alexandre Raphael Cabral all helped to improve the presentation and content of the ms.

Author contribution DC conducted field work, sample collection, and sample preparation, and prepared the ms. MP conducted SEM, EBSD analysis, and data management, and approved the ms**.**

Funding Open Access funding enabled and organized by CAUL and its Member Institutions Funding for the research was provided by University of Otago.

Data availability All data are included in this paper and cited references.

Declarations

Conflict of interest The authors declare no competing interests.

References

Ashley P, Craw D, MacKenzie D, Rombouts M, Reay A (2012) Mafic and ultramafic rocks, and platinum mineralisation potential, in the Longwood Range, Southland, New Zealand. NZ J Geol Geophys 55:3–19

Bishop DG, Mildenhall DC (1994) The geological setting of ventifacts and wind-sculpted rocks at Mason Bay, Stewart Island, and Their Implications for Late Quaternary Paleoclimates. NZ J Geol Geophys 37:169–180

Boyle RW (1979) The geochemistry of gold and its deposits. Geol Surv Canada Bull 280:579

Chapman RJ, Banks DA, Styles MT, Walshaw RD, Piazolo S, Morgan DJ, Grimshaw MR, Spence-Jones CP, Matthews TJ, Borovinskaya O (2021) Chemical and physical heterogeneity within native gold: implications for the design of gold particle studies. Mineral Deposita 56:1563–1588

Chapman RJ, Moles NR, Bluemel B, Walshaw RD (2022a) Detrital gold as an indicator mineral. Geol Soc London Spec Publ 516:313–336

Chapman RJ, Craw D, Moles NR, Banks DA, Grimshaw MR (2022b) Evaluation of the contributions of gold derived from hypogene, supergene and surficial processes in the formation of placer gold deposits. Geol Soc London Spec Publ 516:291–311

Chen-Wiegart YK, Wang S, McNulty I, Dunand DC (2013) Effect of Ag–Au composition and acid concentration on dealloying front velocity and cracking during nanoporous gold formation. Acta Mater 61:5561–5570

Cho J-H, Ha H-P, Oh KH (2005) Recrystallization and grain growth of cold-rolled gold sheet. Metall Materials Trans A 36A:3415–3425

Craw D, Kerr G (2021) Physical and chemical evolution of a Pleistocene marginal marine gold paleoplacer deposit, southern New Zealand. Ore Geol Rev 138:104341

Craw D, Youngson JH, Leckie DA (2006) Transport and concentration of detrital gold in foreland basins. Ore Geol Rev 28:417–430

Craw D, Mitchell M, McCann R, Reay A (2013) Compositional variations and morphological evolution in platinum beach placers, southern New Zealand. Mineral Deposita 48:81–97

Craw D, Kerr G, Reith F, Falconer D (2015a) Pleistocene paleodrainage and placer gold redistribution, western Southland, New Zealand. NZ J Geol Geophys 58:137–153

Craw D, Kerr G, Falconer D (2015b) Mineralogy and provenance of auriferous Waimumu Quartz Gravels, Southland, New Zealand. NZ J Geol Geophys 58:281–295

Craw D, McLachlan C, Negrini M, Becker N (2017) Quantification and prediction of bulk gold fineness at placer gold mines: a New Zealand example. Minerals 7:226. https://doi.org/10.3390/min7110226

Crundwell M, Scott G, Naish T, Carter L (2008) Glacial–interglacial ocean climate variability from planktonic foraminifera during the Mid-Pleistocene transition in the temperate Southwest Pacific, ODP Site 1123. Palaeogeog Palaeoclim Palaeoecol 260:202–229

Cullen DJ (1967) The submarine geology of Foveaux Strait. NZ Oceanographic Inst Mem. 33, Wellington, pp 67

Doherty RD, Hughes DA, Humphreys FJ, Jonas JJ, Juul Jenson D, Kassner ME, King WE, McNelley TR, McQueen HJ, Rollett AD (1997) Current issues in recrystallisation: A review. Materials Sci Eng A238:219–274

Erlebacher J, Aziz MJ, Karma A, Dimitrov N, Sieradzki K (2001) Evolution of nanoporosity in dealloying. Nature 410:450–453

Eyles N (1990) Glacially derived, shallow-marine gold placers of the Cape Yakataga district, Gulf of Alaska. Sed Geol 68:171–175

Garnett RHT (2000) Marine placer gold, with particular reference to Nome, Alaska. In: Cronan DS (ed) Handbook of marine mineral deposits. CRC Press, Boca Raton, pp 67–101

Garnett RHT, Bassett NC (2005) Placer deposits. Econ Geol 100th Anniv vol, p. 813–843

Guisti L (1986) The morphology, mineralogy, and behaviour of "fine-grained" gold from placer deposits of Alberta: sampling

and implications for mineral exploration. Can J Earth Sci 23:1662–1672
Henley RW, Adams J (1979) On the evolution of giant gold placers. Trans Inst Min Metall 88:B41–B50
Holzing A, Frimmel HE, Voland V, Dremel K, Zabler S, Minter WEL (2015) The cover of Mineralium Deposita's anniversary volume uncovered. Mineral resources in a sustainable world. 13th SGA Biennial Meeting 2015. Proceedings, 4: 1407–1410
Hou B, Keeling J, Van Goen B (2017) Geological and exploration models of beach placer deposits, integrated from case-studies of southern Australia. Ore Geol Rev 80:437–459
Hui H, Xia R, Li J, Mei Q, Ma Y, Chen F, Lei Y (2018) Effects of cold rolling and annealing prior to dealloying on the microstructure of nanoporous gold. Nanomaterials 8:540
Kerr G, Falconer D, Reith F, Craw D (2017) Transport-related mylonitic ductile deformation and shape change of alluvial gold, southern New Zealand. Sed Geol 361:52–63
Knight JB, Morison SR, Mortensen JK (1999) The relationship between placer gold particle shape, rimming and distance of fluvial transport; as exemplified by gold from the Klondike District, YukonTerritory, Canada. Econ Geol 94:635–648
Kungurova VE (2021) Evaluating the effectiveness of fine gold extraction technologies on the example of titanomagnetite beach placers of the western coast of Kamchatka. J Mining Inst 252:840–853
Malloch K, Kerr G, Craw D (2017) Placer gold in the Cretaceous Blue Spur Conglomerate at Waitahuna, southern New Zealand. NZ J Geol Geophys 60:239–254
Masson FX, Beaudoin G, Laurendeau D (2022) Multi-method 2D and 3D reconstruction of gold grain morphology in alluvial deposits: a review and application to the Rivière du Moulin (Québec, Canada). Geol Soc London Spec Publ 516:337–352
McClenaghan MB, Paulen RC (2018) Application of till mineralogy and geochemistry to mineral exploration. In: Past glacial environments, 2nd Edition. Elsevier, pp 689–751. ISBN 978-0-08-100524-8
McClenaghan MB, Cabri LJ (2011) Review of gold and platinum group element (PGE) indicator minerals: methods for surficial sediment sampling. Geochem: Explor Environ Anal 11:251–263
McLachlan C, Negrini M, Craw D (2018) Gold and associated minerals in the Waikaia placer gold mine, Northern Southland, New Zealand. NZ J Geol Geophys 61:164–179
Nikiforova Z (2021) Criteria for determining the genesis of placers and their different sources based on the morphological features of placer gold. Minerals 11:381–404
Nikiforova ZS, Gersaimov BB, Tulaeva EG (2011) Genesis of gold-bearing placers and their possible sources (Eastern Siberian Platform). Lith Mineral Res 46:17–29
Nolze G (2015) Euler angles and crystal symmetry. Crystal Res Technol 50:188–201
Prior DJ, Boyle AP, Brenker F, Cheadle MC, Day A, Lopez G, Peruzzo L, Potts GJ, Reddy S, Spiess R (1999) The application of electron backscatter diffraction and orientation contrast imaging in the SEM to textural problems in rocks. Am Mineral 84:1741–1759
Prior DJ, Mariani E, Wheeler J (2009) EBSD in the earth sciences: applications, common practice and challenges. In: Electron backscatter diffraction in materials science: 2nd Edition. Eds Schwartz AJ, Kumar M, Adams BL, Field DP, Springer. Chapter 29, pp. 345-357. ISBN: 978-0-387-88135-5
Reznik VP, Fedorunchuk NA (2000) Microscopic gold in marine and oceanic sediments. Lith Mineral Res 35:311–318
Ritchie T, Scott J, Craw D (2019) Garnet compositions track longshore migration of beach placers in western New Zealand. Econ Geol 114:513–540
Shuster J, Lengke M, Marquez-Zavalia MF, Southam G (2016) Floating gold grains and nanophase particles produced from the biogeochemical weathering of a gold-bearing ore. Econ Geol 111:1485–1494
Stewart J, Kerr G, Prior D, Halfpenny A, Pearce M, Hough R, Craw D (2017) Low temperature recrystallisation of alluvial gold in paleoplacer deposits. Ore Geol Rev 88:43–56
Townley BK, Hérail G, Maksaev V, Palacios C, De Parseval P, Sepulveda F, Orellana R, Rivas P, Ulloa C (2003) Gold grain morphology and composition as an exploration tool: application to gold exploration in covered areas. Geochem: Expl Environ Anal 3:29–38
Turnbull IM, Allibone AH (2003) Geology of the Murihiku area. Inst Geol Nuclear Sci 1:250 000 Geological map 20. Lower Hutt
Upton P, Craw D (2016) Coeval emplacement and orogen-parallel transport of gold in oblique convergent orogens. Tectonophysics 693, Part B: 197–209
Youngson JH (2005) Diagenetic silcrete and formation of silcrete ventifacts and aeolian gold placers in central Otago, New Zealand. NZ J Geol Geophys 48:247–263
Youngson JH, Craw D (1999) Variation in placer style, gold morphology, and gold particle behavior down gravel bed-load rivers: an example from the Shotover/Arrow-Kawarau-Clutha river system, Otago, New Zealand. Econ Geol 94:615–634